Drying Mechanisms in Plasticized Latex Films: Role of Horizontal Drying Fronts

Véronique Divry, Axel Gromer, Mohammad Nassar, C. Lambour, Dominique Collin, Yves Holl

THE JOURNAL OF PHYSICAL CHEMISTRY B

Article

Drying Mechanisms in Plasticized Latex Films. Role of Horizontal Drying Fronts

Véronique Divry, Axel Gromer, Mohammad Nassar, Christophe Lambourg, Dominique Collin, and Yves Holl

J. Phys. Chem. B, **Just Accepted Manuscript** • DOI: 10.1021/acs.jpcb.6b03009 • Publication Date (Web): 31 May 2016

ACS Publications

The Journal of Physical Chemistry B is published by the American Chemical Society. 1155 Sixteenth Street N.W., Washington, DC 20036

Drying Mechanisms in Plasticized Latex Films. Role of Horizontal Drying Fronts

V. Divry, A. Gromer, M. Nassar, C. Lambourg, D. Collin, Y. Holl*

CNRS-ICS & Université de Strasbourg
23, rue du Loess BP 84047
67034 Strasbourg Cedex 2
France

ABSTRACT

This paper presents studies on drying kinetics of latexes with particles made softer and softer by increasing amounts of plasticizer, in relation to speeds of horizontal drying fronts and particle deformation mechanisms. Global drying rates were measured by gravimetry and speeds of horizontal fronts by video camera and image processing. Particle deformation mechanisms were inferred using the deformation map established by Routh and Russel. This required precise measurements of rheological properties of the polymers by the use of a piezorheometer. Results show that latexes with softer particles dry slower but, in our systems, this is not due to skin formation. A correlation could be established between global drying rates and speeds of horizontal fronts, interpreted in terms of evolution of mass transfer coefficients of water in the different areas of the drying system. Speeds of horizontal drying fronts were compared to the Routh and Russel model. A qualitative agreement of the curve shapes was observed that is already remarkable. However, the fit cannot be considered as good. All this appeals to further research efforts in modelling and simulation.

* yves.holl@unistra.fr +333 88 41 41 16

INTRODUCTION

As already apparent in the title and abstract, this paper deals with the complex phenomenon of film formation from a polymer colloid (latex). Research in this field started a long time ago. From a historical point of view, it would be interesting to track back the earliest scientific works on the topic. Routh and coworkers[1] quote a paper published as early as in 1936 about the problem of surfactant distributions in latex films.[2] Older contributions probably exist, but are not easy to accede to.

The mechanism of film formation from a latex is classically divided in three main steps: i) concentration by water evaporation; ii) particle deformation; iii) particle coalescence through chain interdiffusion. These events are cited in a sequential order although they often overlap in time. In some cases, additional steps can be distinguished like crystallization in the liquid state[3, 4] or rupture of the more hydrophilic shell phase before coalescence of the hydrophobic cores.[5] It has to be noted that the drying process can encompass the three main steps. Among the hundreds of papers existing on the general mechanisms of latex film formation, it is advisable to the reader entering the field to start with excellent reviews[6, 7] or nicely-written introductions of some articles (reference 8 is a recent example). Nowadays, even if recent contributions still exist,[9] research in the third main step (coalescence) is less active. Most of the latest published papers deal with drying in relation to particle deformation, and this is also the subject of our article.

Drying might be considered as a trivial and old topic because basic laws (Clausius, Clapeyron) date from the nineteenth century. In reality, drying of complex fluids like colloids is extremely complicated because of coupled phenomena of transport of matter and heat associated to stress development and relaxation over a wide range of characteristic length scales, from the molecular to the macroscopic levels. Again, colloid drying has been reviewed

several times. Let us quote the following ones by Erbil[10], Routh[11], Thiele[12] and Starov and coworkers[13], all worth reading.

A general characteristic of colloid drying is that, except in rare cases, it is heterogeneous. Soon after drying started, zones in the deposit contain less water than others, separated by more or less diffuse interfaces called drying fronts, moving in various directions at different speeds. Figure S1. (in Supporting Information) shows a schematic of a latex during drying. Drying fronts separate drier zones on top and edges and wetter zones at the bottom in the center of the deposit, moving from top to bottom in the normal (vertical or z direction) or in the lateral direction (horizontal or x or y directions). In general, lateral drying fronts move much faster than vertical ones because the mechanisms at the origin of these fronts are different in nature. In both cases, drier zones appear when particle convection overpasses diffusion, i.e. when the Peclet number (precisely defined later in the text) is larger than unity. However, in the vertical direction, convection is solely due to the water – air interface moving towards the substrate upon water loss, whereas, in the horizontal direction, a stronger convection occurs, due to a "capillary pumping effect"[7] of the edges when they are thinner than the center and thus concentrate faster and reach the state of particle close packing.

Then arises the question of particle deformation. On the drier side of a drying front, the polymer concentration progressively increases, reaches close packing at volume fractions around 0.6 or 0.7 and, depending on the particle softness, particle start to lose their spherical shape in such a way that the volume fraction goes above 0.7 and tends towards 1. Obviously, when polymer volume fraction increases much in a zone of a drying system, water transport through this zone might be impeded and drying slowed down. A very pertinent parameter was introduced by Routh and Russel,[14] noted $\bar{\lambda}$,defined as the ratio of the drying rate over the strain rate. Low values of $\bar{\lambda}$ occur when drying is slow compared to deformation and

inversely. This parameter was extensively used in the recent literature on latex film formation. Its usefulness will appear more clearly below, in the discussion of our results.

A fundamental question remains unclear about latex drying. It is the relationship between the global drying rate and the respective speeds of the drying fronts in the vertical and horizontal directions, in relation with the particle strain rate on the dry side of the drying fronts. It is commonly admitted[8] that the main reason for drying slowing down is the formation of a layer on top of a film where the polymer volume fraction is high, a process referred to as "skin formation". The role of horizontal drying fronts is insufficiently questioned. The purpose of our work was to start shedding light on this aspect.

The paper is organized as follows. The first section deals with global drying rates established by the classical way of gravimetric measurements on latexes where particles become softer and softer after addition of increasing amounts of plasticizer (Texanol^{TM}). Then measurements of viscoelastic properties of the more or less plasticized polymers are presented. It allowed us to infer particle deformation mechanisms thanks to the use of the Routh and Russel deformation map.[14] Next, the question of skin formation is discussed. In our systems, it seems that skin formation only plays a minor role. More important is the effect of lateral drying. Our data on horizontal drying fronts are shown in the last section. Speeds of these fronts could be measured and compared to the existing model developed by Routh and Russel in the late nineties.[15, 16]

MATERIALS AND METHODS

Latexes

Five core-shell latexes were synthesized. The particles are composed of random copolymers of butyl acrylate (BuA), methyl methacrylate (MMA) and acrylic acid (AA). The five latexes differ by the percentage of acrylic acid in the composition (either 1 or 2.5 wt%) and the mean

particle diameter (30, 100 or 200 nm). They allowed us to study size and acrylic acid concentration effects on global drying rates (including in mixtures of different particle sizes). In order not to lengthen this paper too much, all size and AA concentration effects are detailed elsewhere.[17] Here, only results concerning the latex of 200 nm with 1 wt% of AA (designated as 200-1), more or less plasticized, will be presented.

The monomers, butyl acrylate (Sigma-Aldrich, purity ≥99%), methyl methacrylate (Merck), acrylic acid (Merck), the surfactant, sodium dodecyl sulfate (SDS, A.C.S Reagent, Sigma Aldrich, purity >99%) and the initiator, sodium persulfate ($Na_2S_2O_8$, reagent grade, Sigma Aldrich, purity ≥98%) were used as received. Distilled water was used throughout synthesis and dialysis. The latex syntheses were performed by semi continuous emulsion polymerization, in a double-wall glass reactor under argon atmosphere. The monomer ratio was calculated using the Fox equation to reach a glass transition temperature (Tg) of the polymers around 35°C. The conversion was higher than 95%. More details about synthesis can be found in reference 18. After synthesis, the latexes were purified by dialysis using a Millipore membrane until the conductivity of water in contact with the latex was less than 3µS/cm. Purification allows elimination of water soluble impurities (residual salts, oligomers and surfactants). After dialysis, the solids content of the latexes was adjusted to around 26% and the pH to 10.0 by dropwise addition of a NaOH solution. The latexes remained stable after purification thanks to the high concentration of acrylic acid in the shell and high pH.[18]

Latexes were characterized by measurements of solids content (gravimetry), mean particle size, particle size distribution and zeta potential (dynamic light scattering), Tgs of the wet and dried latexes (modulated differential scanning calorimetry, MDSC). The viscosity of the latexes was measured with a Haake Mars rheometer (cone plate geometry) and compared to the viscosity calculated with the Mooney equation. Table 1 summarizes the main characteristics of the latex 200-1.

Table 1. Main characteristics of the latexes (without and with Texanol™) used in this study

Latex	Composition (%BuA/%MMA/%AA)	Mean particle diameter	Solids content (±0.5%)	Tg film/dispersion (±1°C)	Zeta Potential * (±1mV)	Measured Viscosity ** (±0.5mPa.s)	Calculated Viscosity ***
200-1	33.3/65.7/1.0	206 nm	25.8%	44°C/31°C	-54 mV	2.5 mPa.s	2.9 mPa.s

* Measured at pH 10. ** Measured at 25°C, σ = 10N. *** Calculated using Mooney equation.

Dispersion	200-1	+6%Tex	+10%Tex	+33%Tex
Initial quantity of Tex compared to solids content /volatile content	/	6.0% / 2.0%	10.0% / 3.3%	33.0% / 10.0%
Tg of the dispersion (± 1°C)	31°C	15°C / 46°C	14°C/45°C	Non measurable
Tg of the dried dispersion (± 1°C)	44°C	23°C	18°C	Below -10°C
Plasticized Polymer Tg*	/	28°C	17°C	-26°C
MFFT*	30°C	14°C	3°C	-40°C

* Calculation based on the Kelley-Bueche equation.[19]

Formulation

As plasticizer (or coalescing agent), we used the well-known Texanol™ (2,2,4-trimethyl-1,3-pentanediol monoisobutyrate) (called Tex in the remainder of the text). It was purchased from Eastman and used as received (purity 98.5 wt% minimum). Plasticized latexes were prepared by adding different amounts of Tex to the latex 200-1. Latex samples containing 6, 10 and 33 wt% Tex based upon the solids content were prepared. The resulting dispersions were allowed to equilibrate at room temperature under stirring before use. The Tgs were measured before and immediately after drying using MDSC. Two Tgs were found for the +6%Tex and +10%Tex. The Tgs of the plasticized polymers and the minimal film formation temperatures (MFFT) of the dispersions were calculated using the Kelley-Bueche equation and the measured 200-1 MFFT.[19] The characteristics of the dispersions are shown in Table 1.

Drying studies by gravimetry and image processing

Films were prepared on rectangular microscope slides (76 x 26 mm) cleaned overnight in a H_2SO_4 bath, rinsed in water and then in ethanol. A thin layer of polytetrafluoroethylene

(PTFE) (Sprayflon®, Roth) was sprayed around the edges of the slides over a width of 3 mm creating a non wettable rim that confined the latex on a constant area in the central part of the rectangle. A constant volume (1mL) of latex was deposited on the PTFE free part of the slide, ensuring the same film thickness for all samples.

Drying took place under controlled conditions in a Plexiglas box: 23±2°C, 75±2%RH, (RH stands for Relative Humidity, the value of 75% was achieved with saturated NaCl solutions) still air. The weight loss of the film was recorded with a digital microbalance (Mettler Toledo ME103E, precision 0.001g). In order to ensure repeatability, the films were compared by pairs using two balances at the same time in the drying box. Drying times could then be measured within an error range of ± 2.0%. Simultaneously, a video camera recorded the film optical changes during drying. The displacements and velocities of the horizontal drying fronts were measured by image processing (ImageJ). Once dry, the films were stored under the same controlled conditions as for drying.

Piezoelectric Rheometer

The viscoelastic properties of the dry films were investigated by dynamic mechanical analysis (DMA) using a homemade piezoelectric rheometer described in details elsewhere.[20] This device, called a piezorheometer, is a plate-plate rheometer operating with piezoelectric ceramics vibrating in shear mode at very low strain (around 10^{-5}), ensuring measurements in the linear regime. The real and imaginary parts of the complex shear modulus were measured at different temperatures, at frequencies ranging from 0.2Hz to 1000Hz. From series of overlapping frequency dependent curves at different temperatures, master curves could be constructed. For the latex 200-1, the viscoelastic properties were measured on dried heat seal pressed films at 100°C for one hour.

Scanning Electron Microscopy

In order to examine the extent of particle deformation inside of the dry films, a special sample holder was designed and built allowing us to take cryo-SEM images of a cross section. A piece of the film was cut out with a razor blade, fixed in our holder and rapidly plunged into a liquid nitrogen slush (Quorum PT 3010T). After introduction into the preparation chamber, the film was freeze fractured at -150°C with a cooled razor blade under high vacuum, and coated with a thin gold layer. Then, the sample was transferred into the microscope (Hitachi SU 8010) and observed at low temperature (-150°C) with the anticontamination blade at -170°C. The electron acceleration tension was 1 or 10 kV depending on the observed charging phenomena.

RESULTS AND DISCUSSION

Global drying rates

Unplasticized 200-1 latex

Figure 1A. shows the weight loss versus time for the latex 200-1 with various initial particle volume fractions. Quantitative data extracted from these curves are summarized in Table 2.

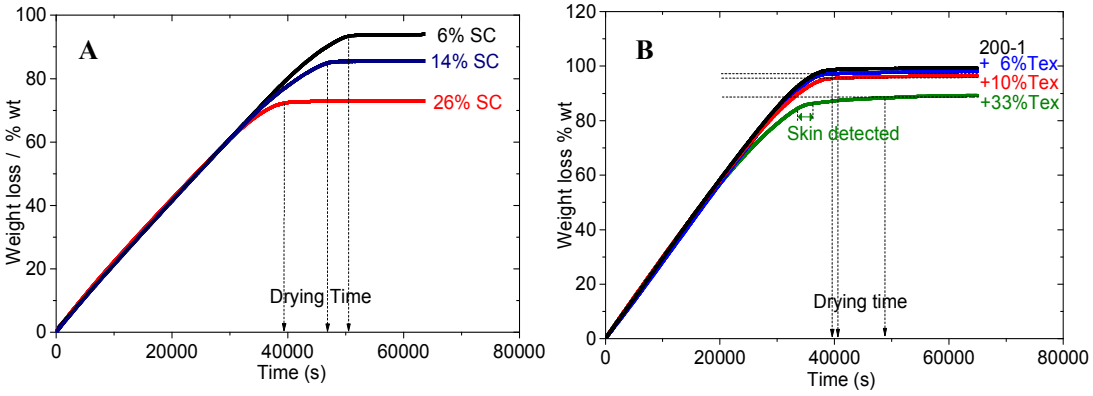

Figure 1. A. Weight loss (in percent of total initial weight of the wet film) versus time for 200-1 with solids contents of 6%, 14% and 26%.
B. Weight loss (in percent of initial weight of water plus Tex) versus time for 200-1 (solids content 26%) with increasing amounts of Tex. Skin formation was detected for 200-1 + 33%Tex as indicated by the green double arrow (see below for comments about this aspect). Drying conditions: 23±2°C, 75±2%RH, still air. Initial film thickness: 770 µm.

The curve shapes are classical: a linear part corresponding to a constant drying rate, in this case identical to the drying rate of pure water ($\dot{E}$ = 1.54 x 10^{-8} m/s in our conditions), followed by a short period (representing here around 20% of the total drying time) where the rate decreases to zero, called the "falling rate period".[21, 22, 23] The total drying time is defined at the first point where the weight loss curve becomes horizontal. For the three latexes with different polymer concentrations, the residual weight closely corresponds the dry content of the initial latex. Although the chemical potential of water and thus the saturated vapor pressure and evaporation rate should decrease with increasing particle concentration, no such effect is experimentally detectable, as also pointed out by other authors.[11] It is interesting to compare the measured total drying time ($t_{dry/exp}$, see Table 2) to a calculated value ($t_{dry/th}$) in a hypothetical case where the latex would dry like pure water, without any effect of the presence of the particles. This leads to a dimensionless drying time, t^*_{dry}, simply defined as $t_{dry/exp}$ / $t_{dry/th}$ with

$t_{dry/th} = \frac{H_0(1-\phi_0)}{\dot{E}}$, H_0 being the initial film thickness, ϕ_0 the initial particle volume fraction and $\dot{E}$ the drying rate. This approach was introduced by Keddie and coworkers.[8] In their paper, t^*_{dry} was comprised between 1.5 and 8. Table 2 shows that, for the latex 200-1 with rigid particles (Tg around 45°C, well above room temperature), t^*_{dry} values are surprisingly close to one. Our latexes almost dry as fast as pure water. It seems that, even when water horizontally recedes below the level of the top particles in a close packed array of non-deformed spheres, it evaporates freely. The observed falling rate would be simply due to the reduced area of the water - air interface when horizontal drying fronts converge towards the center of the film. It is also possible that the cracks appearing in the film during drying much increase the total area of the water – air interface, contributing to the reduction of $t_{dry/exp}$ and t^*_{dry}.

Table 2. Quantitative drying data from gravimetric measurements

Formulation	200-1			+6%Tex	+10%Tex	+33%Tex
Solid content of the formulation	6.0%	14.0%	25.8%	25.4%	25.2%	24.0%
Initial quantity of Texanol compared to the solids / to the volatile content	/	/	/	6.0% / 2.0%	10.0% / 3.3%	33.0% / 10.0%
$t_{dry/th}$ (s)	47000	43000	37100	36526	36526	37037
$t_{dry/exp}$ (s) (± 2.0%)	50580	46860	39330	39620	40620	48850
t^*_{dry} (± 0.02)	1.08	1.09	1.06	1.08	1.11	1.32
Final weight loss %wt compared to the initial volatile content	100%	99.9%	99.2%	97.9%	96.5%	89.3%

Plasticized 200-1 latexes

Figure 1B. shows the weight loss versus time for the latex 200-1 with various concentrations of plasticizer. Quantitative data extracted from these curves are summarized in Table 2.

Curves in Figure 1B. are similar in shape to those in Figure 1A. with a linear part at the drying rate of pure water and a falling rate. The relative importance of the falling rate period increases with the Tex content: 22%, 26%, 31% and 56% for 0%, 6%, 10% and 33% Tex, respectively. The total drying time ($t_{dry/exp}$) increases with increasing Tex concentration, by around 25% going from 0 to 33wt% Tex. The residual weight corresponds here to the part of the volatile content (water plus Tex) of the initial latex that was not evaporated within 6 to 8 hours after the weight apparently stabilized. An analysis of data in Table 2 seems to indicate that very little, if any, Tex is evaporated during latex drying and even a small amount of water is retained within the film. This has a strong influence on mechanical properties of freshly dried films.[17] Besides the increasing importance of the falling rate, another characteristic of the drying behavior of Tex containing latexes is that they progressively deviate from the model of free evaporation of water, as seen in the increase of t^*_{dry}. One can state that increasing the softness of the polymer particles decreases the global drying rate. As drying

rate is most often correlated to particle deformation, let us consider now the deformation mechanisms.

Particle deformation mechanisms

In the literature,[7] five different particle deformation mechanisms were identified: wet sintering, dry sintering, capillary deformation, receding water front, Sheetz deformation. The mechanisms differ by the driving forces for deformation (polymer/water or polymer/air interfacial tension, Laplace pressure at the water-air interface, residual water as pendular rings around particle contacts, continuous polymer layer at the surface). The generalization of the theories for the deformation mechanisms developed by Routh and Russel (RR)[14, 24] allows one to predict the main deformation mechanism taking place during latex drying. In their model, RR assumed that the polymer was a viscoelastic fluid with a single relaxation time (Maxwell fluid). They defined a dimensionless group $\bar{\lambda}$:

$$\bar{\lambda} = \frac{\eta_0 R_0 \dot{E}}{\gamma_{wa} H_0} \quad (1)$$

which is the time for film compaction ($\frac{\eta_0 R_0}{\gamma_{wa}}$) divided by the evaporation time $\frac{H}{\dot{E}}$, with η_0 the polymer zero shear viscosity, R_0 the mean particle radius, γ_{wa} the water-air surface tension, H_0 the initial film thickness and $\dot{E}$ the evaporation rate. When $\bar{\lambda}$ is small, drying is slow compared to deformation and inversely. RR used the Peclet number, $Pe = H_0 \dot{E} / D_0$, with D_0 the Stokes Einstein diffusion coefficient of the particles, to predict vertical inhomogeneities of particle distributions during drying. Finally, they established a map in the $\bar{\lambda} - Pe$ space and so showed where each deformation mechanism would apply. For instance, this map predicts the formation of a skin at the top surface of the latex during drying when $\bar{\lambda} < 1$ (wet sintering: deformation of particle in the wet state) and when $Pe > 1$ (non-uniform drying in the z direction). The most crucial physical quantity in this model is η_0, the polymer zero shear

viscosity. This model is in good agreement with various literature results.[14, 38] Recently, it was further validated experimentally by Carter et al.[8] with the extrapolation of rheological data using the Williams-Landel-Ferry (WLF) equation. However, such an extrapolation may lead to differences in shear viscosities by several orders of magnitude.[14] Simon et al.[25] determined the viscoelastic properties of the polymer by dynamic mechanical analysis in order to measure η_0. They found significant differences between the predicted deformation mechanisms and the experimental results. Carter et al [8] and Simon et al.[25] used NMR profiling techniques to measure the water concentration in the film and to assess the deformation mechanisms. However, Simon et al. results are globally less accurate (low spatial resolution and longtime measurements). In this case, skinning phenomena of a few micrometers are not easily detected and the deformation mechanisms can be mistaken. In the following, we assume that experimental evidences given by Routh and Russel,[24] Gonzalez et al.,[38] Carter et al.[8] are convincing enough to validate the model and we use it as it is.

In order to determine the influence of Tex on particle deformation, dynamic mechanical tests were performed on the dried films to measure η_0 and, knowing the Pe number, the deformation mechanisms were predicted using the RR deformation map. For a viscoelastic fluid (Maxwell model), η_0 is equal to the polymer relaxation time λ multipled by the high frequency shear modulus G_∞. However, classical models such as that of Maxwell cannot fully describe the viscoelastic behavior of polymers[26, 27] because several relaxation mechanisms can occur. One can think of local motions, segmental motions related to the main glass-to-rubber transition, Rouse-Zimm modes, reptation… Therefore, polymers exhibit a broad spectrum of relaxation times. Only average relaxation times can be determined from viscoelastic data. Figure 2A. shows the frequency dependence of the storage modulus G', and the loss modulus G'' for 200-1. The curves were obtained by master curve construction with a temperature dependent shift factor a_T at a reference temperature of 23°C.

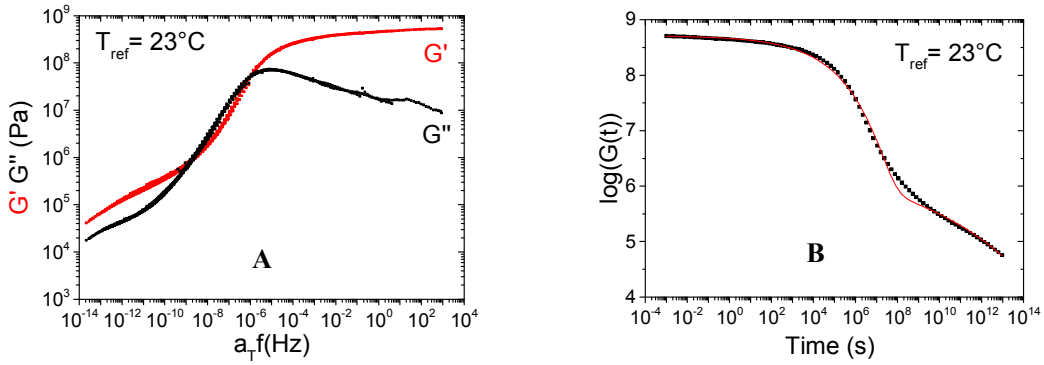

Figure 2. **A**. Frequency dependence of storage (G') and loss (G'') moduli for the film 200-1 at the reference temperature of 23°C. Measurements performed on a continuous film prepared by drying a 200-1 latex and annealing the close packed particles at 100°C.
B. Time dependence of shear modulus $G(t)$ for the film 200-1 at $T_{ref} = 23°C$. The solid line represents the KWW fit.

Two relaxation regions can be differentiated in Figure 2A. The high frequency part of the curve is attributed to segmental motions related to the glass-to-rubber transition. On the low frequency side of the curve, the interpretation is less easy. No simple rubbery plateau is seen but rather a broad relaxation spectrum in G' and G" probably due to a mixture of different relaxation mechanisms like reptation and more local modes. A sophisticated way of determining average relaxation times in these regions was used by Simon et al.[25] Following them, the experimental data in the frequency domain were fitted by a sum of 50 Maxwell relaxations:

$$G^*_{Maxwell}(\omega) = G_\infty \sum_k a_k \frac{\lambda_k \omega}{\lambda_k \omega - i} \qquad (2)$$

No justification for the choice of 50 relaxation times can be found in their paper. However, according to Winter et al.[28, 29] this number should not be taken arbitrarily. It should be large enough to lead to good fits, but not too large to avoid overfitting and artefact generation. The criterion recommended by Winter is to use around 1.5 – 2 modes per decade. With 50 modes for 18 decades, we are close to this range.

Figure 2B. shows the time domain representation of $G^*_{Maxwell}(\omega)$, the shear modulus $G(t)$:

$$G(t)_{Maxwell} = G_\infty \sum_k a_k \exp(^{-t}/_{\lambda_k}) \quad (3)$$

with $a_k > 0$ at a reference temperature of 23°C. The $G(t)$ curve is fitted by a sum of two stretched exponential functions (Kohlrausch-Williams-Watts : KWW):

$$G_{KWW}(t) = G_{\infty,1} \exp\left(-\left(\frac{t}{\lambda_{KWW,1}}\right)^{\beta_1}\right) + G_{\infty,2} \exp\left(-\left(\frac{t}{\lambda_{KWW,2}}\right)^{\beta_2}\right) \quad (4)$$

where $\lambda_{KWW,1}$ and $\lambda_{KWW,2}$ are the two average characteristic relaxation times for the high and low frequency relaxation mechanisms, respectively. β_1 and β_2 measure the broadness of the relaxation time distribution for the two processes ($1 \geq \beta_1, \beta_2 > 0$). $G_{\infty,1}$ and $G_{\infty,2}$ are the high frequency ($\omega \to \infty, t \to 0$) shear moduli for the corresponding relaxation mechanisms. The KWW fit is shown in Figure 2B. as a solid line. The fit parameters are as follows:

$G_{\infty,1} = 5.1 \times 10^8$ Pa $\quad \beta_1 = 0.23 \quad \lambda_{KWW,1} = 1.5 \times 10^4$ s

$G_{\infty,2} = 3.2 \times 10^6$ Pa $\quad \beta_2 = 0.08 \quad \lambda_{KWW,2} = 3.0 \times 10^5$ s

Adj. R square : 99.8%

The small values of β_1 and β_2 indicate broad distributions of relaxation times for the two processes. The two KWW functions do not lead to a perfect fit (especially in the frequency region between the two main relaxation processes). However, this acceptable fit supports the assumption of two distinct relaxation mechanisms and provides meaningful fit parameters.

From the two relaxation mechanisms, two shear viscosities could be calculated by: $\eta_1 = G_{\infty,1} \times \lambda_{KWW,1}$ and $\eta_2 = G_{\infty,2} \times \lambda_{KWW,2}$. The apparent viscosity η' measured for $\omega = 1/t_{dry}$ is also another way to accede to a shear viscosity by graphical determination on the viscosity vs frequency curve (not shown) directly accessible from the moduli vs frequency curves in Figure 2A. The particle radius R_0 is taken as 100 nm, the evaporation rate at $1.54 \times 10^{-8} m/s$ (see above), the initial thickness of the latex before drying is $H_0 = 770\ \mu m$ and the water-air surface tension $\gamma_{wa} = 73\ mN/m$. For each measured shear viscosity, the $\bar{\lambda}$

parameter was calculated in accordance with equation (1). The whole procedure was repeated for the 6, 10 and 33% Tex films formed by drying and aged two months at 75%RH and 23°C.

Table 3 summarizes the zero shear viscosities and the corresponding $\bar{\lambda}$ parameters obtained for each latexes. The errors in Table 3 are the relative standard deviations calculated from statistical errors on the best KWW fit. The large error on η_2 (and correlatively on $\bar{\lambda}_2$) is due to the intrinsically complex elastic and flow properties of our polymer due to the overlap of several relaxation mechanisms in the low frequency domain. Our rheological measurements should have provided more experimental points on the low frequency (or long time) side of the curves but this would have required temperatures the sample could not stand. For η', the error is graphically determined. The Peclet number is estimated to be much higher than one, hence the particles deformation mechanisms can be predicted using the Routh and Russel deformation map. Those predictions are indicated in Table 3.

Table 3. Measured shear viscosities and corresponding Routh and Russel $\bar{\lambda}$ parameters for the different latexes (without and with Tex) at the reference temperature of 23°C. The predicted particle deformation mechanisms ($Pe > 1$), using Routh and Russel deformation map, are indicated in the last line.

Latex	200-1	6%Tex	+10%Tex	+33%Tex
Viscosity (Pa.s)				
η_1 (±25%)	$7.7 \cdot 10^{12}$	$2.1 \cdot 10^{10}$	$6.4 \cdot 10^{8}$	$3.5 \cdot 10^{4}$
η_2 (±1 decade)	$9.6 \cdot 10^{11}$	$6.6 \cdot 10^{9}$	$2.4 \cdot 10^{8}$	$2.0 \cdot 10^{6}$
η' ($\omega = 1/t_{dry}$) (±8%)	$2.4 \cdot 10^{12}$	$2.3 \cdot 10^{11}$	$2.4 \cdot 10^{9}$	$\sim 1.0 \cdot 10^{8}$
$\bar{\lambda}_1$ (±25%)	$2 \cdot 10^{2}$	0.6*	$2 \cdot 10^{-2}$	$1 \cdot 10^{-6}$
$\bar{\lambda}_2$(±1 decade)	$3 \cdot 10^{1}$	0.2*	$7 \cdot 10^{-3}$	$6 \cdot 10^{-5}$
$\bar{\lambda}$ (η') ((±8%))	$7 \cdot 10^{1}$	6	$7. 10^{-2}$	$3 \cdot 10^{-3}$
Predicted deformation mechanism	Receding water front	Capillary deformation	Wet sintering*	Wet sintering*

* Skinning and Sheetz deformation

In Table 3, it can be seen that whatever the three different ways of calculating the viscosity, the predicted mechanism stays globally the same for all four systems. This is true despite the quite large relative standard deviations on $\bar{\lambda}$ (imperfect KWW fits). This result strengthens the viscosity calculation approaches.

Without Tex the predicted deformation mechanism is receding water front.

Figure 3 shows cryo-SEM pictures of the bulk of the dried 200-1 film aged one day (a) and three months (b). The circles in the figure indicate the particle average size of 200 nm. In (a), the particles are only partially deformed after drying. In (b), they have obviously continued their deformation during ageing. In the frame of the receding water front mechanism, this further deformation would be through dry sintering.[30] However, ageing taking place at high relative humidity (75%), plasticizing of the hydrophilic shells probably facilitates the deformation. Intersticial condensed water in the contact areas between particles (moist sintering) may also contribute.[31, 32]

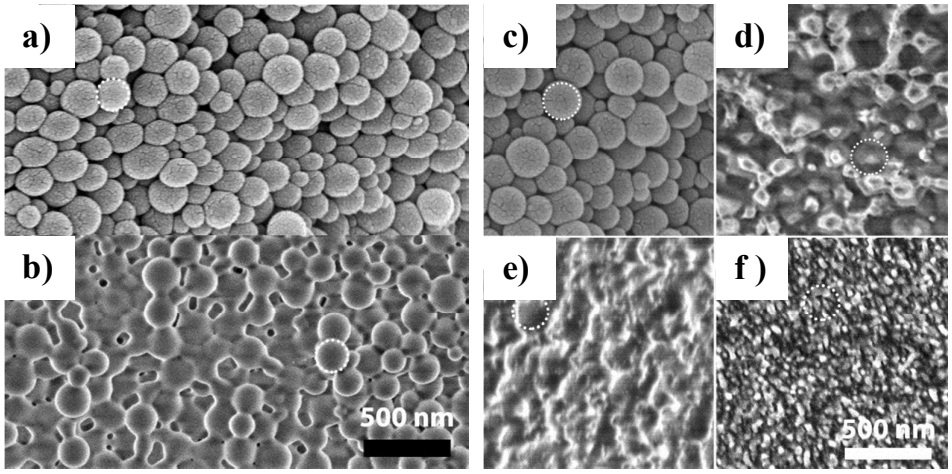

Figure 3. To the left: cryo-SEM images of dried 200-1 films aged one day (a) or three months (b).
To the right: cryo-SEM pictures of dried 200-1 (c) again, for comparison with the three other pictures; 200-1 + 6%Tex (d); 200-1 + 10%Tex(e); 200-1 + 33%Tex (f) aged one day. The pictures are taken into the bulk of the films. The white dotted circles indicate a size of 200 nm.

With Tex, the predicted deformation mechanisms are capillary deformation and wet sintering with skinning and Sheetz deformation (the question of skinning will be further addressed in the next section). The particles deform faster than water evaporates when the concentration in Tex increases.

Figure 3B. shows cryo-SEM pictures of dried 200-1 (c), 6% (d), 10% (e) and 33%Tex (f) films aged one day. The pictures were taken in the bulk of the films. One can see that an

increase of Tex results in more complete particle deformation. With 6%Tex, the particles can still be observed but with flat contact areas. With 10%Tex no particles can be distinguished, only some forms still have the initial particle size. Finally, the 33%Tex film is homogeneous and no particles or forms are observed. The white dots in (f) may be due to the fracture of the film.[33] Those images illustrate the role of a coalescing aid. They are in agreement with the predicted deformation mechanisms. An increase of Tex in the latex modifies the particle deformation mechanisms. This will have some consequences on vertical and horizontal drying, as will be discussed in the following paragraphs.

Skin formation

It is common belief in the film formation community that slowing down of drying is essentially due to skin formation. Particles first accumulate at the water - air interface due to the "snow plow effect" [34] of the interface moving down toward the substrate simply because of evaporation of water ("top-down drying"[34]). Then, if not redispersed by diffusion and soft enough, they can deform (and possibly coalesce) forming a more or less efficient barrier (a skin) hindering further water evaporation. Reference to skin formation is old[35] and many other publications speak of it.[7, 8, 36, 37, 38] The questions to be raised at this point: is there formation of a skin in our systems, when, and to what extent does it contribute to the slowing down of drying? Although several techniques have been used to provide evidence for skin development,[7] like cryo-SEM[39] or SAXS[40], the most efficient and powerful one is certainly Magnetic Resonance Profiling (MRP),[41] as has been demonstrated many times by Keddie and coworkers.[8, 34] Having not access to MRP, we had to look for another approach. Simulations were used also to get some information about skin formation, either using Brownian dynamics[42] or Monte Carlo techniques.[43] Thus, we decided to run the simulation recently developed in our group[44] in the particular case of the 200-1 system (rigid particles). This simulation consists of dividing real space into cells and applying local physical laws to

account for exchanges of matter between neighboring cells. It allows us to accede to particle concentration profiles during drying for various systems, under different conditions. In addition, we used "a poor man technique" called needle pick test[37] consisting of gently touching the surface of the dispersion from time to time during drying. The presence of a skin could be detected by film fragments sticking to the needle. Although coarse, this procedure provides a rough idea of the time when a significant skin starts to form.

Before formation of a skin, particles have to accumulate at the water – air interface. This happens when the Peclet number is high (significantly above 1). Using the simplest definition of the Peclet number in our context,[14] (recalled in the preceding paragraph) and our data for 200-1 (see above), we find Pe = 5.5. Actually, the Stokes Einstein diffusion coefficient is a relevant value only in the dilute regime. At an initial volume fraction of 26%, it is only a rough approximation. Using DWS (Diffusing Wave Spectroscopy),[17] we were able to measure an accurate diffusion coefficient, namely $D = 7.\ 10^{-14}$ m^2/s. With this new value, the Peclet number raises to 166. Furthermore, in our systems, particles are highly repulsive: the zeta potential is high (-54 mV, see Table 1) and the ionic strength low, leading to an initial Debye length of 2.9 nm. As the latex dries, the ionic strength increases, decreasing the Debye length to a final value of 0.2 nm (see Supporting Information, Figure S2). Taking all these data into account, the evolution of the vertical distribution of particles was simulated (Figure 4). The results show that, as expected with a high Pe, particles soon accumulate at the latex – air interface. However, being highly repulsive, they do not come into contact but rather tend to form an array of non-touching particles over the whole thickness (see curve at time 0.93). Only later, as evaporation further decreases the inter particle distance, do they eventually overcome repulsion (which also tends to decrease as drying proceeds) and jump into contact in the final evaporation stages. This vision of the process is consistent with the fact that, for the 200-1 latex, drying follows the model of free evaporation of water.

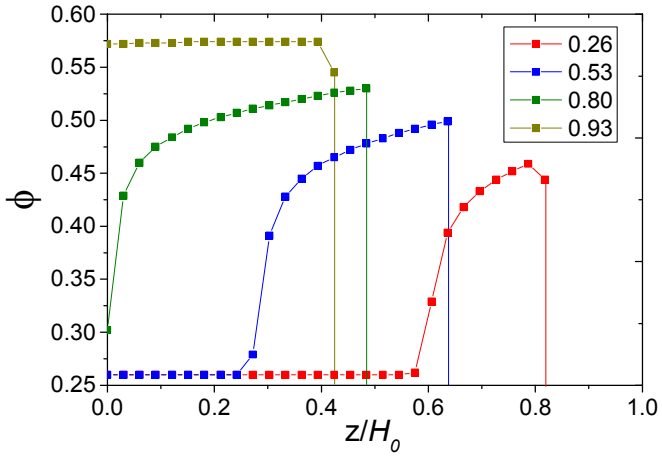

Figure 4. Particle volume fraction of the 200-1 latex versus dimensionless thickness (z or vertical direction) (H_0 is the initial film thickness) at various drying times (time 1 when close packing, $\phi = 0.64$, is reached over the whole thickness). The film-air interface is to the right, the substrate to the left. Pe = 166. ζ = -54 mV. Initial κ^{-1} = 2.9 nm. Initial film thickness: 770 µm.

In the case of latexes containing Texanol, we could not run our simulation because our software is not yet ready for soft repulsive particles. However, rigid or soft, all particles in our systems have the same zeta potential and are subject to the same ionic strength (these values are not significantly affected by the presence of the plasticizer). Thus, particle distributions shown in Figure 4 also apply to latexes with softer particles. This leads to the conclusion that skin formation can only take place late in the drying process. In order to get an additional piece of information about this question, needle pick tests were performed. No skin formation was detected for 200-1 + 6% Tex and 200-1 + 10% Tex. Only for 200-1 + 33%Tex a skin appeared at the time indicated in Figure 1B. close to the horizontal drying fronts and progressively gained the whole fluid zone. If looking at the coordinates of the center of the double arrow, it can be stated that skin appears at a time corresponding to 72% of the total drying time, when 96% of the evaporable compounds are already eliminated. In other words, after skin formation, 28% of the total drying time is needed to get rid of the last 4% of volatiles. Obviously, skin formation is not sufficient to account for slowing down of drying,

which, in that particular case of the 200-1 + 33%Tex latex, starts when 44% of the total drying time has elapsed.

These considerations illustrate that predictions of the RR deformation model have to be taken with some care. For the 10% Tex containing latex, the prediction of skinning and Sheetz deformation is not confirmed. And, for 33% Tex, skinning occurs only very late in the process. This is because the RR model does not take into account the case of highly repulsive particles.

Horizontal drying fronts

Figure 5 presents pictures of the latexes 200-1 and 200-1 + 10% Tex during drying. Horizontal drying fronts are clearly visible, as already observed a long time ago by many authors, starting with Hwa in the 1960s.[45] Videos of the whole drying process for both latexes can be found in the Supporting Information Section. The first front, called particle front, separates a fluid, white zone from a blue one where the particles are close packed (red line marked 1 in the pictures). The blue color is attributed to the fact that the objects scattering visible light are no longer polymer particles like in the fluid zone but the interstices between particles, here full of water.[46] In the latex 200-1, particles do not significantly deform. A second front separates the blue zone from a third zone also white in color where cracks can be seen (blue line marked 2). This second front is called "water front". The third, white zone is considered dry. It is white and not blue because the scattering object is now air with a different refractive index from water. In the plasticized latex 200-1 + 10% Tex, the third zone is not white but transparent (black on the picture because the transparent film substrate is placed onto a black paper) (blue line marked 2') and this second front is called an optical clarity front. Particles are deformed forming a medium with no strong scatterers inside. The interpretations of the different colors are based on MRP experiments by Keddie et al.[47] and

cryo-SEM by Scriven and coworkers.[39] The later team proposes a well-illustrated example of horizontal drying fronts for ceramic containing latexes in reference 48.

The displacement of the fronts was followed versus time (Figure 5). For 200-1, the first front (particle front) starts slowly and progressively accelerates. The second front is much delayed and quickly vanishes, almost at the same time as the first one. The final state is a white deposit with many cracks (see Supporting Information). The video also shows that the particle front is slower along y (width of the rectangle) than along x. The reason for this is not clear at this point. For 200-1 + 10% Tex, the first front has almost the same behavior as for 200-1 but the second one (optical clarity front) starts sooner and closely follows the particle front, leading to a blue zone of almost constant width. At the end, the film is transparent. A central crack appears along x, due to non-totally relaxed stresses or to a partial dewetting phenomenon. Qualitatively, the latexes with 6% and 33% Tex behave like 200-1 + 10% Tex.

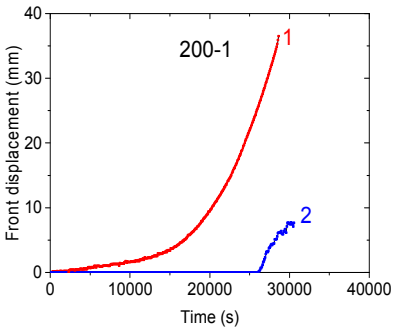

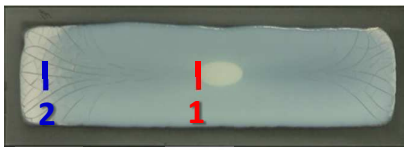

1: Particle front
2 : Water front

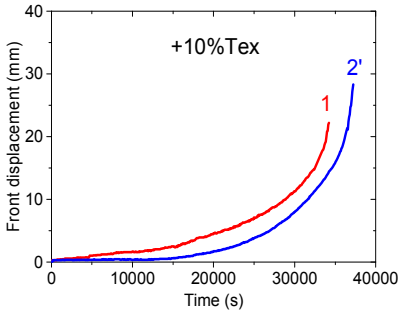

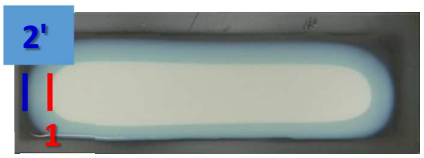

1 : Particle front
2' : Optical clarity front

Figure 5. Displacement (the origin is at the left edge of the deposited latex) of drying fronts versus time for the latexes 200-1 and 200-1 + 10%Tex. Standard drying conditions (23±2°C, 75±2%RH, still air).

Figure 6A. shows the velocity of the first front for the latexes with increasing amounts of plasticizer (0, 6, 10, 33% Tex) versus time. The tendency of the fronts to accelerate is clear in all cases, although much more marked for the unplasticized latex. Increasing the amount of Tex decreases the velocity of the particle front, but 200-1 + 10% Tex and 200-1 + 33% Tex have very similar velocities.

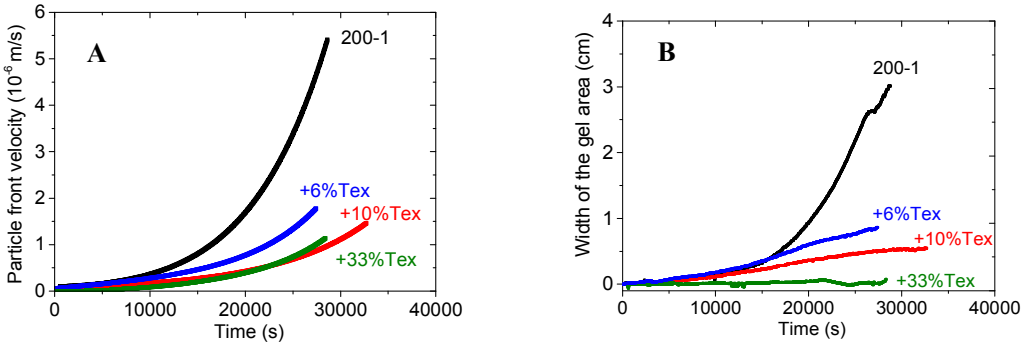

Figure 6. A. Velocity of the first drying front (particle front) versus time for the latexes with increasing amounts of plasticizer. Curves were smoothed by fitting with a stretched exponential. **B**. Width of the gel area versus time for the latexes with increasing amounts of plasticizer. Standard drying conditions.

A first explanation for the front acceleration is that the front moves inwards because particles are conveyed to the edges by the water flux due to the capillary aspiration by the close packed area where water continues to evaporate. The central fluid zone being more concentrated as drying proceeds, more and more particles arrive at the front (also called a compaction front by some authors) and make it move more rapidly. Another point is that the aspiration strength of the close packed area (which can also be called a "wet gel") depends on its width and porosity. In the porous medium constituted by the gel, there is a competition between capillarity which sucks the fluid and flow hindering by porosity (Darcy's law accounts for this flow reduction). A ratio of these two effects, called reduced capillary pressure, was introduced by RR[15] to account for this competition (see also reference 7 and Supporting Information for more details):

$\bar{p} = \frac{10\gamma k_p H_0}{R_0\,\mu \dot{E} L^2}$ with γ = water-air interfacial tension, k_p = permeability of the wet gel, H_0 = initial film thickness, μ = viscosity of the dispersion, R_0 = particle radius, $\dot{E}$ = rate of evaporation, and L a characteristic length (here the capillary length). With non-deformable particles, when this ratio reaches one, the capillary pressure is no longer strong enough to drive water further toward the edge and the wet gel transforms into a dry gel, defining the water front (2). With deformable particles, it is more complicated because the permeability of the wet gel is not constant but progressively decreases ($k_p \downarrow$) until closing the total porosity and leading to a transparent film, defining the optical clarity front (2'). As suggested by a referee during the review process, a possible reason for the slowdown of the drying fronts with the addition of Tex is that increased deformation pushes water in the bulk of the film and this lowers the volume fraction in the fluid region. One should note that the transparent zone is not necessarily totally dry just behind the second front. With all these considerations in mind, one can understand that the width of the blue zone should be correlated with the speed of the particle front. Comparing Figure 6A. and Figure 6B. leads to the conclusion that the correlation qualitatively exists, except that the front of 200-1 + 33% Tex is as fast as for 200-1 + 10% Tex whereas it should be slower. This can be attributed to the fact that, for 200-1 + 33% Tex, at the latest drying stages, the particle front becomes blurred and ill-defined, leading to a large uncertainty on the front position and, thus, on the width of the blue zone.

It is also important to stress here that the speeds of the particle front correlate with the global drying rates. For 0, 6 and 10 % Tex, it was shown above that skin formation was not observed. For 33% Tex, a skin formed but only late in the drying process when it was already apparent that this latex dried significantly slower than the previous ones (see Figure 1B.). Thus, it is tempting to state that slowing down in our systems can be attributed, not to skin formation, but to slowing down of the horizontal fronts, due to particle deformation in the wet gel area. In a sense, it may seem paradoxical that slowing down the particle front with the

consequence of decreasing slower the size of the fluid zone, supposed to be the zone which evaporates water at the highest rate, decreases the global drying rate. In fact, looking at the global drying rate imposes to consider all evaporating zones of the film. In our systems without skin formation, the slowing down of the global drying rate is actually attributed to the areas behind the first drying front where water evaporation is hindered.

In general, under given external conditions, the global rate of drying depends on the area of the surface evaporating water and its evolution with time, taking into account a local and time depend mass transfer coefficient representing the difficulty for a water molecule to reach air starting from inside the deposited latex. The knowledge of these mass transfer coefficients in different situations (skins of different thicknesses and permeability, wet gels with more or less deformed particles, transparent zones still containing water) together with water distributions in the system could allow to calculate global drying rates. Such an approach might be accessible to simulation.

Let us now finish this paragraph about horizontal drying fronts by a comparison between experimental results and theoretical predictions by the RR model.

Comparison of experimental speeds of drying fronts with theoretical predictions

Routh and Russel designed a theoretical model for horizontal fronts propagating through drying latex films.[15, 16] This model was experimentally validated by Keddie's team using MRP.[47] A summary of the main features of the model can be found in the Supporting Information Section associated to this paper. We have compared our experimental results for the positions of the drying fronts versus time with this model. The drying process was considered only up to the time when close packing was reached in the whole film. In plotting the experimental data, like in reference 16, we considered average positions obtained by equating the areas of the fluid and wet gel domains to disks. The front position and time were scaled using the experimental values of the evaporation rate and initial film height, and

assuming a surface tension of water of 73 mN/m, and a viscosity of the dispersion of 1 Pa.s (again like in reference 16). With these values, the capillary length in our systems is approximately 2.5 cm.

In order to calculate the theoretical front positions, the equations of the model were solved with a computer program using the finite difference method. For this purpose, the latex film was divided into 100 spatial steps and the time step was chosen in order to insure the stability of the integration method. It was assumed that the film had an initial height H_0 with a rounded edge (a piece of an ellipse) extending up to $\bar{x} = 1$ ($\bar{x} = 0$ corresponds to the film edge) and that a small gel region of size: $\bar{x}_{gel} = 0.001$ was formed initially at the film edge. Different edge shapes were tried and the same behavior as in references 15 and 16 was observed: shallower edges (equivalent to lower contact angles) increased the velocity of the particle front. Ignoring the exact contact angle in our systems but considering that the latex rather well wets the hydrophilic glass surface, a low value was chosen. Moreover, we estimated that $\phi_{max} = 0{,}69$ based on image analysis of particle packing in cryo-SEM images (a similar choice was made in reference 47). We assumed non-deformable particles when simulating the system without coalescing agent. According to our experimental conditions, and assuming: $\mu = 1$ mPa.s, we should get a maximum value of the reduced capillary pressure: $\bar{p} \sim 27$. However for such a value, no water front appeared. Instead, a lower value: $\bar{p} = 17$ was chosen, so that the water front appears approximately at the same time as in the experiment. We assumed deformable particles when simulating the systems with plasticizer. In this case, values of lambda based on DMA results were taken (Table 3), i.e., $\bar{\lambda} = 7$ for the latex with 6% Tex, and $\bar{\lambda} = 0.2$ for the latex with 10% Tex.

The results of the comparison are shown in Figure 7. It should be noted that, for 200-1 and 200-1 + 6% Tex, the final time approximately matches that predicted by theory (~ 0.58), whereas it is significantly longer for 200-1 + 10% Tex due to the longer falling rate period in

this sample. Although general shapes and behaviors roughly agree, the fit is far from good. In particular, the experimental fronts seem to move at a slower pace than predicted. There are several possible sources of discrepancy between theory and experiment. One could be the limited size of our samples and their geometry which differs significantly from the semi-infinite film described in the model. Another source of discrepancy is the fact that $Pe > 1$ in our systems, thus the vertical particle distribution is not homogeneous, whereas the RR model assumes $Pe = 0$. Then, it should be noted that, in the model, the velocities of the fronts are sensitive to the shape of the initial height profile, however this shape is not known precisely in our experiments. As mentioned before, the maximum capillary pressure we used is lower than that calculated from experimental data. Previous work already pointed at the difficulty to determine the experimental value of the capillary pressure precisely.[47] In addition, cryo-SEM images suggest that the particles are in fact not completely non-deformable. In Figure 7, for 0% and 6% Tex, the optical clarity fronts appear at approximately the same time as found experimentally, validating the values taken for $\bar{\lambda}$. For 10% Tex, the discrepancy is large suggesting that particles are not as soft as expected, in other words that the value of $\bar{\lambda}$ is underestimated.

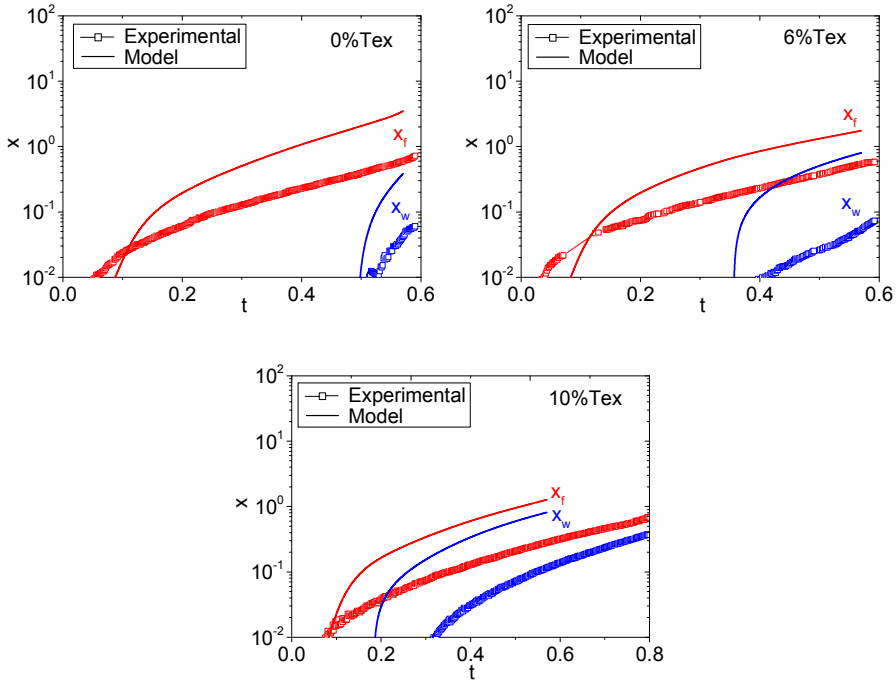

Figure 7. Position of the drying fronts (X_f particle front, X_w water front) vs time: comparison of experimental values (squares) and Routh and Russel model (solid lines). Systems: 200-1, 200-1 + 6% Tex, 200-1 + 10% Tex, as indicated in the figures. Time is scaled on a characteristic time: $\frac{H_o}{\dot{E}}$, and horizontal distances are scaled on the capillary length (see Supporting Information for details).

One could argue that the level of agreement between theory and experiment is sensitive to the value taken for the low shear viscosity of the dispersion. A lower viscosity will result in a larger capillary length, thus the shift of the front line will be towards shorter adimensional distances, i.e., the level of agreement between experiment and theory will be worse. In order to improve the agreement, we should instead increase the viscosity. As pointed out in reference 16, the value that was chosen (1 Pa.s) is somewhat arbitrary. It seemed unrealistic to us to go above 1 Pa.s, at least in the first stages of drying. As drying proceeds, the viscosity of the dispersion increases. To give better agreement, the model needs to be improved in the future in order to include a volume fraction dependent viscosity. One could also argue that optical clarity could occur at volume fractions lower than one and, again, this will alter the numerical predictions. Indeed, if the volume fraction is lowered, the theoretical curves for 6% and 10% Tex are shifted downwards, improving the agreement. However, the value of volume fraction corresponding to optical clarity cannot be pushed too low. We checked that, for a value of 0.95, the improvement was negligible.

It looks like the model about speeds of drying fronts, in spite of its high degree of sophistication, is still based on assumptions that conduct it rather far from reality.

CONCLUSION

In order to manipulate the global drying rate of a colloid, obviously, the most efficient way is to adjust the external parameters: temperature, humidity, air flux. However, this is not always possible, for example for road or building paints. Under given external conditions, the drying rate depends on a complex interplay between heterogeneities developing in various directions (top-down and edge-in drying[34]). These phenomena of heterogeneous drying depend on the nature and properties of the colloid, essentially the rate at which particles can deform under the various possible deformation driving forces.

Let us summarize the main outcomes of our study. When particles are mostly rigid at the drying temperature, the latex almost dries like free water, like if particles were absent. It was known before that the influence of rigid particles is small but the extent of the analogy with free water observed in our systems was a surprise. When particles become progressively softer, as expected, drying slows down. Obviously, there is a correlation between this slowing down and particle deformation. To gain information about the evolution of the deformation mechanisms when particle softness increases, the Routh and Russel (RR) model was applied, considering that it was validated enough by experimental studies (although some disagreements can be found in the literature[25]). This supposes a rather sophisticated analysis of polymer viscoelastic properties, performed thanks to an original piezoelectric rheometer. As expected, the RR $\bar{\lambda}$ parameter (drying rate over particle deformation rate) decreases when particles get softer. The corresponding deformation mechanisms could be inferred using the RR deformation map. With the techniques available in our environment, it was not easy to

address the question of skin formation. A combination of simulation and macroscopic testing of the surface characteristics of the latex during drying (needle pick test) led us to the conclusion that significant skinning only occurs for our softer system, late in the drying process. With this, it was demonstrated that drying slowing down is not always due to skin formation. Afterwards, a study of horizontal drying fronts was undertaken. The speeds of horizontal drying fronts increase with time upon drying. They decrease when particles get softer, in conjunction with decreasing global drying rates. Interpretations of front speeds in terms of capillary flux hindered by porosity and tortuosity of the concentrated zone on the edge side of the drying system (wet gel) that can be found in the literature are qualitatively validated by our work. To be more quantitative, our experimental results were confronted to theoretical calculations based on the RR model. Although in general agreement as far as curve shapes are concerned, the calculations do not really fit the experimental points. This appeals to model refinements based on less severe assumptions.

What are the ways of improvement of this kind of drying studies? Trying to improve existing experimental techniques in terms of resolution and response time is an always ongoing option. It might also be possible to imagine new methods. Being able to accede to local drying rates (in the fluid, in the wet gel, in the transparent zones) at all time during drying would lead to a highly valuable piece of information. An idea that could be tested would be to observe the drying latex with an IR camera and relate the local temperature fluctuations to local drying rates. This supposes a fine knowledge of the thermal properties of the materials (heat capacities, thermal conductivities and diffusivities, heat transfer coefficients) and, probably, a highly complex modelling of heat exchanges but it might be worth trying. And, besides experiments, modelling and simulation are promising approaches. Efforts in simulation are pursued in our research group.

Supporting Information available:

- Scheme of a drying latex

- Decrease of Debye length during drying

- Videos of the drying of the unplasticized and plasticized latexes

- Horizontal drying fronts: comparison with RR model

ACKNOWLEDGEMENTS

We gratefully acknowledge helpful discussions with Dr. L. Ruhaut, Mr. F. Pagnac and Mr. J.L. Vincent (SAR Company). Many thanks to Dr. M. Schmutz for the cryo-SEM images and Mr. J. Iss for technical assistance (computer interfacing). The financial support to the PhD work of one of us (V.D.) by the French Company "Société d'Applications Routières" (SAR) is gratefully acknowledged.

REFERENCES

(1) Gundabala, V.R.; Zimmerman, W.B.; Routh, A.F. A Model For Surfactant Distribution in Latex Coatings. *Langmuir* **2004**, *20*, 8721–8727.

(2) Wagner, H.; Fischer, G. Filmbildung und Emulsionen. *Kolloid Zeitschrift*. **1936**, 77, 12-20.

(3) Dosho, S.; Ise, N.; Ito, K.; Iwai, S.; Kitano, H.; Matsuoka, H.; Nakamura, H.; Okumura, H.; Ono, T.; Sogami, I.S.; et al. Recent Study of Polymer Latex Dispersions. *Langmuir* **1993**, *9*, 394-411.

(4) Sosnowski S.; Li L.; Winnik M.A.; Clubb B.; Shivers, R.R. Morphology of Melt-Pressed Latex Films Examined by Scanning and Freeze-Fracture Electron Microscopy. *J. Polym. Sci. B. Polym. Phys.* **1994**, *32*, 2499-2508.

(5) Joanicot, M.; Wong, K.; Richard, J.; Maquet, J.; Cabane, B. Ripening of Cellular Latex Films. *Macromolecules* **1993**, *26*, 3168-3175.

(6) Keddie, J.L. Film Formation of Latex. *Mater. Sci. Eng.* **1997**, *R 21*, 101-170.

(7) Keddie, J.; Routh, A. Fundamentals of Latex Film Formation: Processes and Properties; Springer: Dordrecht. The Netherlands, **2010**.

(8) Carter, F.T.; Kowalczyk, R.M.; Millichamp, I.; Chainey, M.; Keddie J.L. Correlating Particle Deformation with Water Concentration Profiles during Latex Film Formation: Reasons That Softer Latex Films Take Longer to Dry. *Langmuir* **2014**, *30*, 9672−9681.

(9) Pohl, K.; Adams, J.; Johannsmann, D. Correlation Between Particle Deformation Kinetics and Polymer Interdiffusion Kinetics in Drying Latex Films. *Langmuir* **2013**, *29*, 11317−11321.

(10) Erbil, H.Y. Evaporation of Pure Liquid Sessile and Spherical Suspended Drops: a Review. *Adv. Colloid Interface Sci.* **2012**, *170*, 67–86.

(11) Routh, A. F. Drying of Thin Colloidal Films. *Rep. Prog. Phys.* **2013**, *76*, 46603 (30pp).

(12) Thiele, U. Patterned Deposition at Moving Contact Lines. *Adv. Colloid Interface Sci.* **2014**, *206*, 399–413.

(13) Kovalchuk, N.M.; Trybala, A.; Starov, V.M. Evaporation of Sessile Droplets. *Curr. Opin. Colloid Interface Sci.* **2014**, *19*, 336–342.

(14) Routh, A.F.; Russel, W.B. A Process Model for Latex Film Formation: Limiting Regimes for Individual Driving Forces. *Langmuir* **1999**, *15*, 7762-7773.

(15) Routh A.F.; Russel W.B. Horizontal Drying Fronts During Solvent Evaporation From Latex Films. *AICHE J.* **1998**, *44*, 2088-2098.

(16) Routh, A.F.; El-Aasser, M.S.; Tang, J.; Russel, W. Process Model for Latex Film Formation: Optical Clarity Fronts. *J. Coat. Technol.* **2001**, *73/916*, 41-48.

(17) Divry, V. Formation Mechanisms and Structure / Property Relationships in Fast Drying Latex Films. Ph.D. Thesis, University of Strasbourg, France, **2016**.

(18) Belaroui, F.; Hirn, M.P.; Grohens, Y.; Marie, P.; Holl, Y. Distribution of Water-Soluble and Surface-Active Low-Molecular-Weight Species in Acrylic Latex Films. *J. Colloid Interface Sci.* **2003**, *261*, 336-348.

(19) Toussaint, A.; De Wilde, M.; Molenaar, F.; Mulvihill, J. Calculation of Tg and MFFT Depression Due to Added Coalescing Agents. *Prog. Org. Coat*. **1997**, *30*, 179-184.

(20) Collin, D., Covis, R.; Allix, F.; Jamart-Grégoire, B.; Martinoty, P. Jamming Transition in Solutions Containing Organgelator Molecules of Amino-Acid Type: Rheological and Calorimetry Experiments. *Soft Matter*, **2013**, *9*, 2947-2958.

(21) Croll, S.G. Drying of Latex Paint. *J. Coating Technol*. **1986**, *58 (734)*, 41-49.

(22) Croll, S.G. Heat and Mass Transfer in Latex Paints During Drying. *J. Coating Technol.* **1987**, *59 (571)*, 81-92.

(23) Narita, T.; Hébraud, P.; Lequeux, F. Effects of the Rate of Evaporation and Film Thickness on Nonuniform Drying of Film-Forming Concentrated Colloidal Suspensions. *Eur. Phys. J. E* **2005**, *17*, 69−76.

(24) Routh, A.F.; Russel, W.B. Deformation Mechanisms During Latex Film Formation: Experimental Evidence. *Ind. Eng. Chem. Res.* **2001**, *40*, 4302-4308.

(25) Simon, F.; Kunkel, S.; Oehler, H.; Lellinger, D.; Spahn, P.; Alig, I. Investigation of Deformation Mechanisms During Latex Film Formation by Combination of Unilateral NMR and Near Infrared Measurements. *Prog. Org. Coat.* **2010**, *70*, 230-239.

(26) Ferry, J.D. Viscoelastic Properties of Polymers. J. Wiley & Sons, **1980**.

(27) Toussaint, A.; De Wilde, M. A Comprehensive Model of Sintering and Coalescence of Unpigmented Latexes. *Prog. Org. Coat.* **1997**, *30*, 113-126.

(28) Baumgaertel, M.; Winter, H.H. Interrelation Between Continuous and Discrete Relaxation Time Spectra. *J. Non-Newtonian Fluid Mech.* **1992**, *44*, 15-36.

(29) Winter, H.H. Analysis of Dynamic Mechanical Data: Inversion into a Relaxation Time Spectrum and Consistency Check. *J. Non-Newtonian Fluid Mech.* **1997**, *68*, 225-239.

(30) Keddie, J.L.; Meredith, P.; Jones, R.A.L.; Donald, A.M. Kinetics of Film Formation in Acrylic Latices Studied with Multiple-Angle-of-Incidence Ellipsometry and Environmental SEM. *Macromolecules* **1995**, *28*, 2673-2682.

(31) Lin F.; Meier D.J. A Study of Latex Film Formation by Atomic Force Microscopy. 1. A Comparison of Wet and Dry Conditions. *Langmuir* **1995**, *11*, 2726-2733.

(32) Lin F.; Meier D.J. A Study of Latex Film Formation by Atomic Force Microscopy. 2. Film Formation vs Rheological Properties: Theory and Experiment. *Langmuir* **1996**, *12*, 2774-2780.

(33) Ge, H.; Zhao, C.L.; Porzio, S.; Zhuo, L.; Davis, H.T.; Scriven, L.E. Fracture Behavior of Colloidal Polymer Particles in Fast-Frozen Suspensions Viewed by Cryo-SEM. *Macromolecules* **2006**, *39*, 5531-5539.

(34) König, A.M.; Weerakkody, T.G.; Keddie, J.L.; Johannsmann, D. Heterogeneous Drying of Colloidal Polymer Films: Dependence on Added Salt. *Langmuir* **2008**, *24*, 7580–7589.

(35) Sheetz, D.P. Formation of Films by Drying of Latex. *J. Appl. Polym. Sci.* **1965**, *9*, 3759-3773.

(36) Mallégol, J.; Bennett, G.; Dupont, O.; McDonald, P.J.; Keddie, J.L. Skin Development During the Film Formation of Waterborne Acrylic Pressure Sensitive Adhesives Containing Tackifying Resin. *J Adhes.* **2006**, *82*, 217-238.

(37) Erkselius, S.; Wadsö, L.; Karlsson, O.J. Drying Rate Variations of Latex Dispersions Due to Salt Induced Skin Formation. *J. Colloid Interf. Sci.* **2008**, *317*, 83–95.

(38) Gonzalez, E.; Paulis, M.; Barandiaran, M.J.; Keddie, J.L. Use of a Routh−Russel Deformation Map to Achieve Film Formation of a Latex With a High Glass Transition Temperature. *Langmuir* **2013**, *29*, 2044-2053.

(39) Ma, Y.; Davis, H.T.; Scriven, L.E. Microstructure Development in Drying Latex Coatings. *Prog. Org. Coat.* **2005**, *52*, 46–62.

(40) Dingenouts, N.; Ballauff, M. First Stage of Film Formation by Latexes Investigated by Small-Angle X-ray Scattering. *Langmuir* **1999**, *15*, 3283-3288.

(41) Glover, P. M.; Aptaker, P. S.; Bowler, J. R.; Ciampi, E.; McDonald, P. J. A Novel High-Gradient Permanent Magnet for the Profiling of Planar Films and Coatings. *J. Magn. Reson.* **1999**, *139*, 90–97.

(42) Liao, Q.; Chen, L.; Qu, X.; Jin, X. Brownian Dynamics Simulation of Film Formation of Mixed Polymer Latex in the Water Evaporation Stage. *J. Colloid Interface Sci.* **2000**, *227*, 84 −94.

(43) Reyes, Y.; Duda, Y. Modeling of Drying in Films of Colloidal Particles. *Langmuir* **2005**, *21*, 7057−7060.

(44) Gromer, A.; Nassar, M.; Thalmann, F.; Hébraud, P.; Holl, Y. Simulation of Latex Film Formation Using a Cell Model in Real Space: Vertical Drying. *Langmuir* **2015**, *31*, 10983−10994.

(45) Hwa, J.C.H. Mechanism of Film Formation from Lattices. Phenomenon of flocculation. *J. Polym. Sci. A* **1964**, *2*, 785-796.

(46) Schroeder, W.F.; Liu, Y.; Tomba, J.P.; Soleimani, M.; Lau, W.; Winnik, M.W. Effect of a Coalescing Aid on the Earliest Stages of Polymer Diffusion in Poly(Butyl Acrylate-Co-Methyl Methacrylate) Latex Films. *Polymer* **2011**, *52*, 3984-3993.

(47) Salamanca, J.M.; Ciampi, E.; Faux, D.A.; Glover, P.M.; McDonald, P.J.; Routh, A.F.; Peters, A.C.I.A.; Satguru, R.; Keddie, J.L. Lateral Drying in Thick Films of Waterborne Colloidal Particles. *Langmuir* **2001**, *17*, 3202-3207.

(48) Luo, H.; Scriven, L.E.; Francis, L.F. Cryo-SEM Studies of Latex/Ceramic Nanoparticle Coating Microstructure Development. *J. Colloid Interf. Sci.* **2007**, *316*, 500–509.

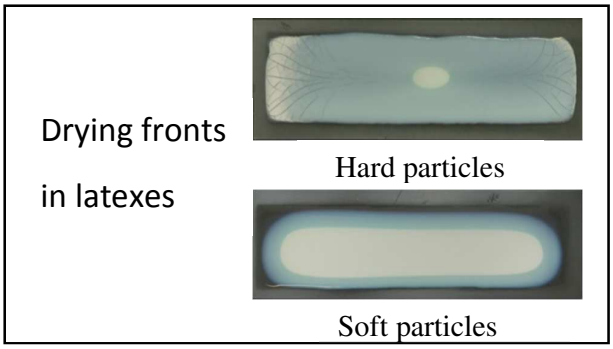
Drying fronts
in latexes
Hard particles
Soft particles